Chinese Chemical Letters 33 (2022) 3999–4002

Contents lists available at ScienceDirect

Chinese Chemical Letters

journal homepage: www.elsevier.com/locate/cclet

Co porphyrin-based metal-organic framework for hydrogen evolution reaction and oxygen reduction reaction

Zuozhong Liang[1,*], Hongbo Guo[1], Haitao Lei, Rui Cao*

Key Laboratory of Applied Surface and Colloid Chemistry, Ministry of Education, School of Chemistry and Chemical Engineering, Shaanxi Normal University, Xi'an 710119, China

ARTICLE INFO

Article history:
Received 7 September 2021
Revised 9 November 2021
Accepted 16 November 2021
Available online 24 November 2021

Keywords:
Molecular catalysis
Hydrogen evolution reaction (HER)
Oxygen reduction reaction (ORR)
Co porphyrin
Metal-organic framework (MOF)

ABSTRACT

Constructing molecule@support composites is an attractive strategy to realize heterogeneous molecular electrocatalysis. Herein, we synthesized metal-organic framework (MOF)-supported molecular catalysts for hydrogen evolution and oxygen reduction reaction (HER/ORR). Ligand exchange strategy was used to prepare molecule@support hybrids due to the same functional group. A series of hybrids were obtained using Co porphyrin (**1**) and different MOFs including MIL-88(Fe), MOF-5(NiCo) and UIO-66(Zr). The **1**@MOF-5(NiCo) had the best HER and ORR activity compared with **1**@MIL-88(Fe) and **1**@MOF-5(NiCo). These hybrids also exhibited tunable selectivity for ORR with four-electron process, which can be attributed to the synergistic effect of porphyrin molecules and MOFs. This work provides a possibility for molecular catalysts to improve activity of HER and tune selectivity of ORR.

Recently, energy-related small molecule activation reactions attracted great attention for sustainable energy utilization and storage [1–6]. Inspired from nature, homogeneous molecular electrocatalysts have attracted great attention for due to their clear molecular structures [7–12]. This feature is beneficial for investigating structure-function relationship and catalytic reaction mechanism to design more efficient molecular catalysts. [13–20]. However, the practical application of molecular catalysts requires transforming homogeneous molecular electrocatalysts into heterogeneous electrocatalysts.

Recently, lots of strategies have been developed to construct heterogeneous electrocatalysts with molecular catalysts [21–26]. On the one hand, molecular catalysts can be constructed into covalent/metal organic frameworks (COFs/MOFs) [27–29]. The stability of these frameworks still remains a great challenge. On the other hand, molecular catalysts can be immobilized on electrode surfaces or proper substrates directly [23-25,30]. First, molecular catalysts can be directly adsorbed on proper substrates such as carbon black, carbon nanotubes and graphene by drop-casting [31]. This strategy usually leads to the aggregation of molecular catalysts. Second, molecular catalysts can be covalently attached to the surface of materials such as Au electrode and carbon nanotube [32–35]. However, this formation of covalent bond between supports and molecular catalysts is very difficult. Third, molecular catalysts can be coordinated to metal-organic framework (MOF) materials such as ZIF-8 and UIO-66 through ligand exchange [36,37]. The ligand exchange is an effective strategy to prepare molecule@MOF hybrids [37–39]. The electrocatalytic activity and selectivity of these hybrids for ORR can be tuned through the synergistic effect by regulating molecules and MOFs [36]. However, rare research has been reported for HER with this kind of hybrid.

Herein, a variety of molecule@MOF composites were prepared with Co 5,10,15,20-tetrakis(4-carboxyphenyl)porphyrin (**1**) as molecular catalyst and one-dimensional (1D) MIL-88(Fe), two-dimensional (2D) MOF-5(NiCo), and three-dimensional (3D) UIO-66(Zr) as MOF supports. Schematic illustration of preparation (ligand exchange) and electrocatalysis (HER and ORR) for Co porphyrin-based MOFs is shown in Scheme 1. We measured the morphology and structure of MOFs and these hybrids systematically. Electrocatalytic hydrogen evolution and oxygen reduction reaction (HER/ORR) were evaluated for these hybrids. These hybrids showed improved activity for HER and selectivity for ORR. With this strategy, diverse molecule@MOF hybrids with different composites, shapes and sizes can be obtained by regulating molecular catalysts and MOFs. This work demonstrates the promising application of molecule@MOF hybrids in energy-related small molecule activation.

First, we prepared several MOFs including MIL-88(Fe), MOF-5(NiCo) and UIO-66(Zr). These MOFs were synthesized from

* Corresponding authors.
E-mail addresses: liangzuozhong@snnu.edu.cn (Z. Liang), ruicao@snnu.edu.cn (R. Cao).
[1] These authors contributed equally to this work.

https://doi.org/10.1016/j.cclet.2021.11.055
1001-8417/

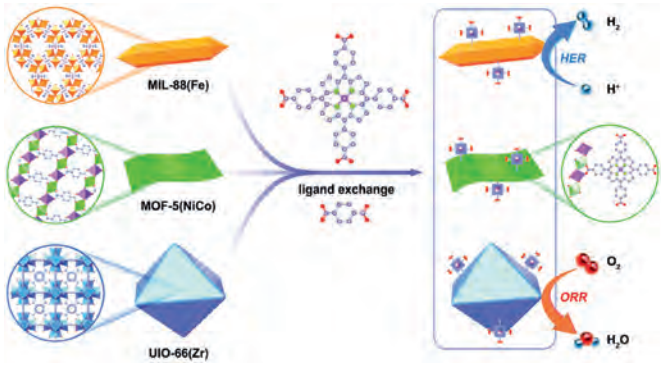

Scheme 1. Schematic illustration of preparation (ligand exchange) and electrocatalysis (HER and ORR) for Co porphyrin-based metal-organic frameworks.

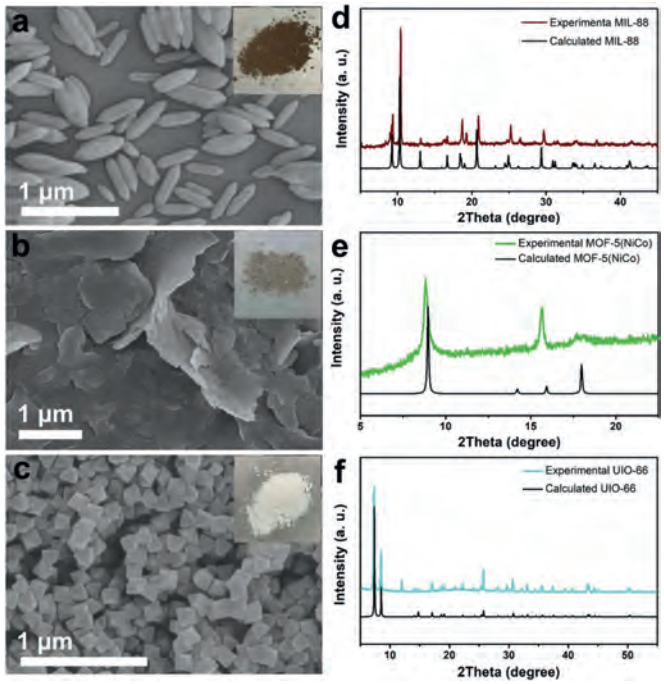

Fig. 1. (a-c) SEM images and (d-f) experimental and calculated XRD patterns of (a, d) MIL-88(Fe), (b, e) MOF-5(NiCo) and (c, f) UIO-66(Zr). Inset: photos of corresponding MOFs.

carboxyl coordinated metals. Fig. 1 shows the color, morphology and structure of as-prepared MOFs. Herein, 1D rod-like MIL-88(Fe) with brown color was prepared (Fig. 1a). The average length of MIL-88(Fe) is about 500 nm. 2D plate-like MOF-5(NiCo) with gray color was obtained (Fig. 1b). 3D octahedral UIO-66(Zr) with white color was synthesized (Fig. 1c). The size of UIO-66(Zr) is about 100 nm. Experimental and calculated XRD patterns confirm the successful preparation of MIL-88(Fe), MOF-5(NiCo) and UIO-66(Zr) (Figs. 1d-f).

Herein, Co porphyrin **1** was selected as model molecular catalyst due to the existence of –COOH group. Co porphyrin **1** was first synthesized according to synthesis procedure shown in Scheme S1 (Supporting informaiton). Mass spectrometry (MS) and nuclear magnetic resonance (NMR) results demonstrate the successful synthesis of Co porphyrin **1** (Figs. S1-S5 in Supporting informaiton). UV–vis curve of **1** shows obvious Soret and Q bands at 428 and 543 nm, respectively (Fig. 2a). Cyclic voltammogram (CV) curve of **1** displays two reversible redox waves of formal Co^{II}/Co^{I} (−1.19 V *vs.* ferrocene) and Co^{I}/Co^{0} (−2.26 V *vs.* ferrocene) (Fig. 2b and Fig. S6 in Supporting informaiton). The linear correlation of Co^{II}/Co^{I} peak

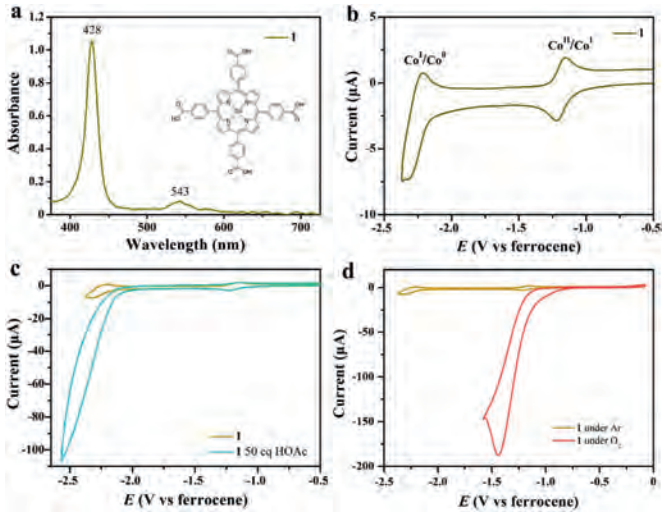

Fig. 2. (a) UV–vis spectrum of Co porphyrin **1** (inset molecule). (b) CV of **1** in acetonitrile with 0.1 mol/L Bu_4NPF_6 under Ar with glassy carbon (GC) electrode. (c) CVs of 0.5 mmol/L **1** under argon and with 25 mmol/L HOAc measured in DMF with 0.1 mol/L $Bu_4N(PF_6)$. (d) CVs of 0.5 mmol/L **1** under Ar and under O_2.

currents and square root of scan rates demonstrates that molecules of **1** can freely diffuse (Fig. S7 in Supporting informaiton). Electrocatalytic HER curve of **1** under Ar with 25 mmol/L of HOAc shows that $Co^{I/0}$ redox wave converted into a catalytic peak (Fig. 2c), attributing to the reduction of protons. Furthermore, the current of catalytic peak increases with increasing of ion concentration (Fig. S8 in Supporting informaiton). As shown in Fig. 2d, CVs of 0.5 mmol/L **1** in DMF under Ar and under O_2 indicate that **1** has the properties of ORR.

Then, molecule@MOF hybrids were synthesized with ligand exchange method. Fig. 3 displays characterization results of these hybrids. According to SEM images of **1**@MIL-88(Fe), **1**@MOF-5(NiCo) and **1**@UIO-66(Zr), morphology of these MOFs still remains after grafting molecules (Figs. 3a-c). Color of these composites shown in inset photos further demonstrates the change of initial surface structures. To further confirm the formation of molecule@MOF hybrids, scanning TEM images and distribution of elements of **1**@MIL-88(Fe) show obvious and uniform distribution of Co, Fe, O, N and C (Fig. 3d). UV–vis spectra of **1** and **1**@MOF-5(NiCo) are shown in Fig. 3e. Obvious characteristic Soret and Q bands were observed, demonstrating the grafting of molecular catalysts on surface of MOFs. Thermogravimetric analysis data of MOFs and **1**@MOF hybrids demonstrate the formation of composites (Figs. S9–11 in Supporting information). To further confirm the stability of structures, XRD patterns of calculated UIO-66 and **1**@UIO-66(Zr) are displayed in Fig. 3f. The main structure of UIO-66 remains after experiencing ligand exchange. High-resolution X-ray photoelectron spectroscopy (XPS) spectra of N 1s, Co 2p and C 1s for these hybrids further confirm the chemical environment of N, Co and C atoms (Fig. S12 in Supporting information), which is consistent with our previous reports [36]. In addition, the molar amount of loaded Co on **1**@MIL-88(Fe) and **1**@UIO-66(Zr) is ~1.0%. The Co content on **1**@MOF-5(NiCo) is unpredictable due to the existence of Co in MOF-5(NiCo). Above all, we obtained molecule@MOF hybrids with porphyrins grafting on MOFs.

To confirm the practical application of these as-prepared molecule@MOF hybrids, electrocatalytic HER and ORR activities were investigated (Fig. 4). The results are listed in Table 1. For HER, **1**@MOF-5(NiCo) has the smallest overpotential with a value of 605 mV at 10 mA/cm^2 compared with **1**@UIO-66(Zr) (630 mV) and **1**@MIL-88(Fe) (692 mV) measured in 0.5 mol/L H_2SO_4 with GC electrode (Fig. 4a). In contrast, Pt/C has an overpotential of 55 mV

Table 1
Performance comparison of **1**@MOF hybrids.

Reaction	Condition	Parameter	**1**@MOF-5(NiCo)	**1**@MIL-88(Fe)	**1**@UIO-66(Zr)
HER	0.5 mol/L H_2SO_4	η (mV) Tafel (mV/dec)	605 −74	692 −94	630 −75
ORR	0.1 mol/L KOH	$E_{1/2}$ (V *vs.* RHE) *n*	0.785 3.6	0.782 3.5	0.781 3.4

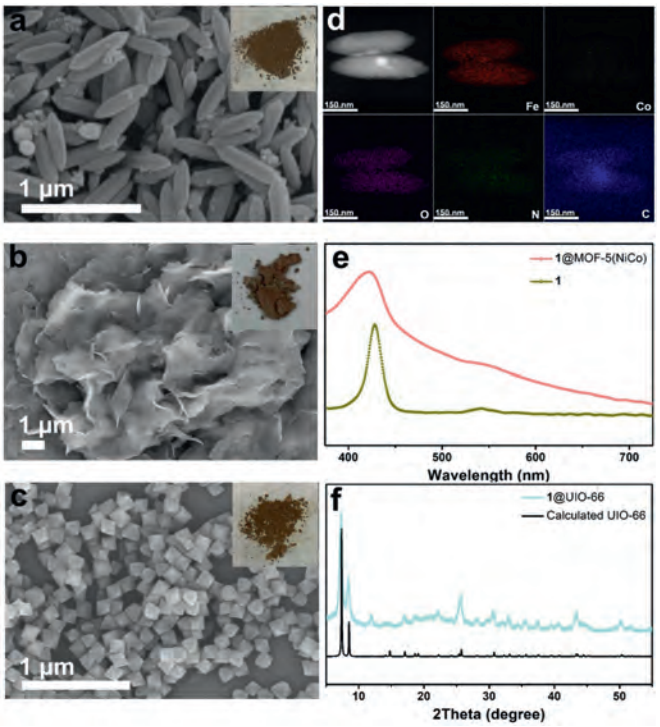

Fig. 3. SEM images of (a) **1**@MIL-88(Fe), (b) **1**@MOF-5(NiCo) and (c) **1**@UIO-66(Zr). (d) Scanning TEM images and distribution of elements for **1**@MIL-88(Fe). (e) UV–vis spectra of **1** and **1**@MOF-5(NiCo). (f) XRD patterns of calculated UIO-66 and **1**@UIO-66(Zr). Inset: photos of corresponding **1**@MOFs.

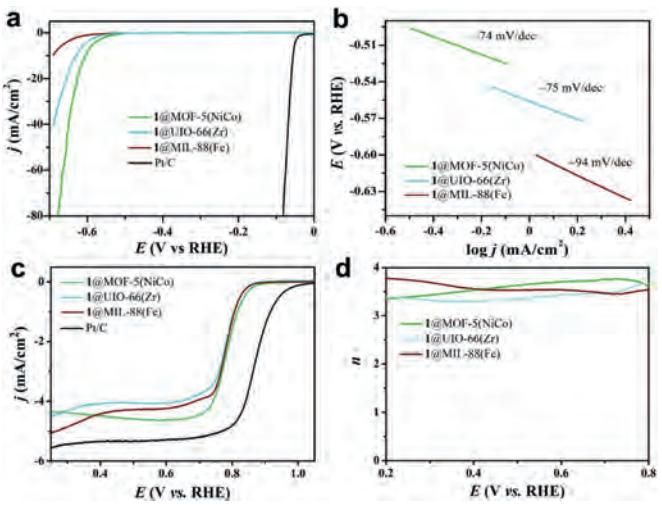

Fig. 4. (a) LSV data and (b) Tafel plots of **1**@MIL-88(Fe), **1**@MOF-5(NiCo), **1**@UIO-66(Zr) and Pt/C measured in 0.5 mol/L H_2SO_4 with GC electrode. (c) LSV data and (d) electron transfer number of **1**@MIL-88(Fe), **1**@MOF-5(NiCo), **1**@UIO-66(Zr) and Pt/C measured in 0.1 mol/L KOH with RRDE electrode.

at the same condition. Tafel slope of **1**@MOF-5(NiCo), **1**@UIO-66(Zr), and **1**@MIL-88(Fe) is 74, 75 and 94 mV/dec (Fig. 4b).

For ORR, the activity and selectivity of Co porphyrin **1** and MOF-5(NiCo) were first measured. The onset potential E_{onset} and half-wave potential $E_{1/2}$ of **1** is ~0.81 V (*vs.* reversible hydrogen electrode, RHE) and 0.74 V (*vs.* RHE), respectively, measured in 0.1 mol/L KOH with rotating ring disk electrode (RRDE) (Fig. S13 in Supporting information). The electron transfer number (*n*) of **1** was also measured and calculated. The **1** has a *n* value of 2.6, demonstrating a 2e ORR process (Fig. S14 in Supporting information). In addition, the E_{onset} and $E_{1/2}$ of MOF-5(NiCo) is 0.67 V (*vs.* RHE) and 0.57 V (*vs.* RHE), respectively (Fig. S15 in Supporting information). The *n* value of MOF-5(NiCo) is ~3.5, demonstrating a 4e ORR process (Fig. S16 in Supporting information). Then, the activity and selectivity of these molecule@MOF hybrids for ORR were measured. The $E_{1/2}$ of **1**@MOF-5(NiCo) is 0.785 V (*vs.* RHE), which is slightly larger than that of **1**@MIL-88(Fe) (0.782 V *vs.* RHE) and **1**@UIO-66(Zr) (0.781 V *vs.* RHE) (Fig. 4c). Furthermore, **1**@MOF-5(NiCo) has a limited current density of 4.6 mA/cm^2, which is larger than that **1**@MIL-88(Fe) (4.1 mA/cm^2) and **1**@UIO-66(Zr) (4.3 mA/cm^2). For comparison, Pt/C has an $E_{1/2}$ of 0.87 V (*vs.* RHE). Electron transfer number of these hybrids was also measured and calculated. All these hybrids experienced 4e ORR process (Fig. 4d). Specifically, **1**@MOF-5(NiCo) has an average *n* value of 3.6, which is larger than that of **1**@MIL-88(Fe) (3.5) and **1**@UIO-66(Zr) (3.4). These results demonstrate the synergistic effect of molecular catalysts and MOFs. The reduced H_2O_2 on the active site of Co porphyrin may experience further reduction on the surface of MOF to realize 4e reduction process for ORR. This result is also consistent with previous reported molecule@MOF hybrids [36]. The controlled potential electrolysis test of hybrid catalysts for HER and ORR further confirm the durability (Fig. S17 in Supporting information). SEM images and high-resolution XPS spectra of these catalysts further confirm the stability of molecule@MOF hybrids (Figs. S18-S20 in Supporting information).

In summary, we report a simple and universal strategy to realize immobilization of molecular catalysts on MOF supports for HER and ORR. Co porphyrin was selected as model molecular catalyst, and 1D MIL-88(Fe), 2D MOF-5(NiCo) and 3D UIO-66(Zr) were selected as MOF supports. Our results demonstrate that **1**@MOF-5(NiCo) exhibits the best HER performance with an overpotential of 605 mV at 10 mA/cm^2 and a Tafel slope of 74 mV/dec measured in 0.5 mol/L H_2SO_4. All molecule@MOF hybrids show similar ORR activity with an $E_{1/2}$ of 0.79 V (*vs.* RHE) measured in 0.1 mol/L KOH. The combination of Co porphyrin and MOFs greatly improves the 4e selectivity of ORR due to the synergistic effect. This work discussed a new kind of porphyrin@MOF electrocatalysts for HER and ORR to transform molecular catalysts into heterogeneous catalysts. This strategy can be also used to develop other hybrid electrocatalysts for other energy-related small molecule activation reactions.

Declaration of competing interest

The authors declare no conflict of interest.

Acknowledgments

We are grateful for support from National Natural Science Foundation of China (Nos. 21808138, 22178213 and 21773146), Fundamental Research Funds for the Central Universities (No. GK202103029), and Young Talent fund of University Association for Science and Technology in Shaanxi, China (No. 20200602).

Supplementary materials

Supplementary material associated with this article can be found, in the online version, at doi:10.1016/j.cclet.2021.11.055.

References

[1] C.X. Zhao, J.N. Liu, J. Wang, et al., Adv. Mater. 33 (2021) 2008606.
[2] C.X. Zhao, J.N. Liu, B.Q. Li, et al., Adv. Funct. Mater. 30 (2020) 2003619.
[3] C.X. Zhao, B.Q. Li, J.N. Liu, Q. Zhang, Angew. Chem. Int. Ed. 60 (2021) 4448–4463.
[4] C.X. Zhao, J.N. Liu, J. Wang, et al., Chem. Soc. Rev. 50 (2021) 7745–7778.
[5] B. Wang, C. Tang, H.F. Wang, et al., Adv. Mater. 31 (2019) 1805658.
[6] T. Cui, J. Dong, X. Pan, et al., J. Energy Chem. 28 (2019) 123–127.
[7] B. Zhang, L. Sun, Chem. Soc. Rev. 48 (2019) 2216–2264.
[8] M.L. Pegis, C.F. Wise, D.J. Martin, J.M. Mayer, Chem. Rev. 118 (2018) 2340–2391.
[9] W. Zhang, W. Lai, R. Cao, Chem. Rev. 117 (2017) 3717–3797.
[10] H. Lei, X. Li, J. Meng, et al., ACS Catal. 9 (2019) 4320–4344.
[11] X.P. Zhang, A. Chandra, Y.M. Lee, et al., Chem. Soc. Rev. 50 (2021) 4804–4811.
[12] X.P. Zhang, H.Y. Wang, H. Zheng, W. Zhang, R. Cao, Chin. J. Catal. 42 (2021) 1253–1268.
[13] X. Guo, N. Wang, X. Li, et al., Angew. Chem. Int. Ed. 59 (2020) 8941–8946.
[14] S. Bhunia, A. Rana, P. Roy, et al., J. Am. Chem. Soc. 140 (2018) 9444–9457.
[15] L. Xie, X.P. Zhang, B. Zhao, et al., Angew. Chem. Int. Ed. 60 (2021) 7576–7581.
[16] C. Costentin, J.M. Savéant, J. Am. Chem. Soc. 140 (2018) 16669–16675.
[17] B. Lv, X. Li, K. Guo, et al., Angew. Chem. Int. Ed. 60 (2021) 12742–12746.
[18] A.C. Brezny, S.I. Johnson, S. Raugei, J.M. Mayer, J. Am. Chem. Soc. 142 (2020) 4108–4113.
[19] Y. Liu, G. Zhou, Z. Zhang, et al., Chem. Sci. 11 (2020) 87–96.
[20] K. Guo, H.T. Lei, X.L. Li, et al., Chin. J. Catal. 42 (2021) 1439–1444.
[21] Z. Liang, H.Y. Wang, H. Zheng, W. Zhang, R. Cao, Chem. Soc. Rev. 50 (2021) 2540–2581.
[22] F. Li, H. Yang, W. Li, L. Sun, Joule 2 (2018) 36–60.
[23] L. Xie, J. Tian, Y. Ouyang, et al., Angew. Chem. Int. Ed. 59 (2020) 15844–15848.
[24] M. Garrido, M.K. Volland, P.W. Münich, et al., J. Am. Chem. Soc. 142 (2020) 1895–1903.
[25] J. Meng, H.T. Lei, X.L. Li, W. Zhang, R. Cao, J. Phys. Chem. C 124 (2020) 16324–16331.
[26] Y. Li, N. Wang, H. Lei, X. Li, R. Cao, Coord. Chem. Rev. 442 (2021) 213996.
[27] M.O. Cichocka, Z. Liang, D. Feng, et al., J. Am. Chem. Soc. 142 (2020) 15386–15395.
[28] B.Q. Li, S.Y. Zhang, B. Wang, et al., Energy Environ. Sci. 11 (2018) 1723–1729.
[29] G. Xu, H. Lei, G. Zhou, et al., Chem. Commun. 55 (2019) 12647–12650.
[30] H. Lei, Q. Zhang, Y. Wang, et al., Dalton Trans. 50 (2021) 5120–5123.
[31] H. Qin, Y. Wang, B. Wang, et al., J. Energy Chem. 53 (2021) 77–81.
[32] S. Gentil, N. Lalaoui, A. Dutta, et al., Angew. Chem. Int. Ed. 56 (2017) 1845–1849.
[33] X. Li, H. Lei, J. Liu, et al., Angew. Chem. Int. Ed. 57 (2018) 15070–15075.
[34] C.J. Kaminsky, J. Wright, Y. Surendranath, ACS Catal. 9 (2019) 3667–3671.
[35] L. Xie, X. Li, B. Wang, et al., Angew. Chem. Int. Ed. 58 (2019) 18883–18887.
[36] Z. Liang, H. Guo, G. Zhou, et al., Angew. Chem. Int. Ed. 60 (2021) 8472–8476.
[37] I. Liberman, R. Shimoni, R. Ifraemov, et al., J. Am. Chem. Soc. 142 (2020) 1933–1940.
[38] T. Zhao, J. Han, X. Jin, et al., Angew. Chem. Int. Ed. 58 (2019) 4978–4982.
[39] D. Yu, Q. Shao, Q. Song, Nat. Commun. 11 (2020) 927.